

Prospects for high-resolution probes of galaxy dynamics tracing background cosmology in MaNGA

Gyeong-Min Lee^a, Maurice H.P.M. van Putten^{1,1},

^a*Physics and Astronomy, Sejong University, 209 Neungdong-ro, 05006, Seoul, South Korea*

Abstract

Large- N galaxy surveys offer unprecedented opportunities to probe weak gravitation in galaxy dynamics that may contain correlations tracing background cosmology. Of particular interest is the potential of finite sensitivities to the background de Sitter scale of acceleration $a_{ds} = cH$, where H is the Hubble parameter and c is the velocity of light. At sufficiently large N , this is possibly probed by ensemble-averaged ("stacked") rotation curves (RCs) at resolutions on par with present estimates of the Hubble parameter H_0 . Here, we consider the prospect for studies using the large N *Mapping Nearby Galaxies at Apache Point Observatory* MaNGA at APO survey. In a first and preliminary step, we consider unbiased control of sub-sample size by consistency in the three Position Angles, θ , from photometry and velocity fields of gas and stars by spectroscopy within 30° . In sub-samples of size $N = N_i(\theta)$, the scatter in-the-mean σ/\sqrt{N} is found to reach one percent levels, differentiated over inclination angle i and θ . In regular propagation of uncertainties, this scatter contributes $\kappa\sigma/\sqrt{N}$ to the standard error in-the-mean to the observable, where κ is determined by the choice of observables. As a lower bound to scatter in stacked RCs, MaNGA hereby appears promising for high-resolution analysis of sensitivity to RCs to background cosmology, notably across a sharp C^0 -transition (van Putten, 2018) of Newtonian to anomalous dynamics across a_{ds} and, further out, the baryonic Tully-Fisher relation. In turn, these markers provide a novel measurement of cosmological parameters.

Keywords: white dwarfs, mass-radius relation, Chandrasekhar

Email address: mvp@sejong.ac.kr (Maurice H.P.M. van Putten)

¹INAF-OAS Bologna via P. Gobetti 101 I-40129 Bologna Italy, Italy

1. Introduction

Galaxy surveys offer avenues to probe weak gravitation pioneered in spiral galaxies by Tully and Fisher (1977). A dramatic extension is the discovery of galaxy formation at cosmic dawn by the *James Webb Space Telescope* (JWST) (e.g. van Putten, 2024b). Modern large- N surveys offer radically new opportunities for high-resolution studies hereof using (sub-)groups of galaxies with relatively homogeneous statistical properties, e.g., observed by dynamics of gas and stars and model fits. For sufficiently large N , this may further allow for binning over different redshifts.

A key question is the feasibility of high-resolution studies with uncertainties on par with modern precision cosmology. High-resolution observations of the evolving Universe on galactic and cosmological scales is a hallmark of modern cosmology with the aim to map the Hubble expansion and structure formation in the Universe across all redshifts (Riess et al., 2022; Tristram et al., 2024).

This development is gradually bringing into view significant departures from the concordance model Λ CDM (Di Valentino et al., 2021), which assumes a constant vacuum energy density Λ and an asymptotic de Sitter cosmology in the distant future. Notably, the expansion history at early and late times reveals a tension in the Hubble constant, in *Planck* Λ CDM-analysis of the *Cosmic Microwave Background* (CMB) (Tristram et al., 2024) and, independently, in the Local Distance Ladder (LDL) (Riess et al., 2022). This H_0 -tension has reached a significance of 5σ by resolving H_0 at statistical uncertainties at about the one percent (Riess et al., 2022; Di Valentino et al., 2021). Hubble expansion consistent with early and late-time cosmology may point to a dynamic dark energy (van Putten, 2025).

In light of this, it is critical to also test Λ CDM for its predictions on sub-horizon scales, in the growth of large scale structure formation (e.g. Jedamzik et al., 2021), the dynamics of galaxy clusters (Zwicky, 1937; Perivolaropoulos and Skara, 2022; Natarajan et al., 2024; Huang et al., 2024), and galaxies dynamics (Rubin and Ford, 1970; Tully and Fisher, 1977; Milgrom, 1983; Famaey and McGaugh, 2012; Lelli et al., 2016; McGaugh et al., 2016; Sanders and McGaugh, 2002; Nestor Shachar et al., 2023).

This suggests the need for one-percent precision studies of galaxy dynamics - a standard error-in-the mean of about 1% in large- N ensemble-averaged observables. Such can then be used to study potentially subtle correlations of galaxy dynamics with the cosmological background, hitherto hinted at using relatively small- N surveys (van Putten, 2018). To study this potential model-independently in some generality, we here set out to quantify consistency in photometric-spectroscopic data of spiral galaxies by some canonical statistics to be specified further below.

Photometric observations provide extensive morphological classification of galaxy dynamics (Hubble, 1927; Maslej-Krešňáková et al., 2021; Ndung'u et al., 2023; Medina-Rosales et al., 2024). Spectral energy distributions (SED) by multi-wavelength observations further provide detailed probes of a variety of properties such as the Initial Mass Function (IMF) of stars and star formation rates (SFR) and mass-to-light ratios M/L (Salpeter, 1955; Bell and de Jong, 2001; Brinchmann et al., 2004; Madau and Dickinson, 2014; Zhang et al., 2024), essential to the direct measurement of baryonic matter content. For spiral galaxies, the well-established Tully-Fisher relation (TFR, Tully and Fisher (1977)) stands out, revealing anomalous galaxy dynamics based on baryonic matter content alone (bTFR, McGaugh et al. (2000); McGaugh (2012)).

In late-time cosmology, the physical origin of bTFR is ambiguous, however, arising from dark matter conform Λ CDM or non-Newtonian dynamics in departure thereof. In contrast, Λ CDM is up-ended at cosmic dawn by JWST ‘Impossible galaxies’, when dark matter is already maximal (van Putten, 2024b). The bTFR and the ultra-high redshift JWST galaxy may have a potentially unified origin in a finite sensitivity of galaxy dynamics, including galaxy formation at cosmic dawn, to the background de Sitter scale of acceleration (van Putten, 2017a, 2024b,a).

$$a_{dS} = cH, \quad (1)$$

where c is the velocity of light and H is the Hubble parameter.

Detailed studies of the bTFR by modern large N galaxy surveys resolve galaxy rotation curves by high-resolution spectroscopy in the footsteps of the first pioneering Doppler shift observations (Slipher, 1915). This is realized by long-slit observations, providing one-dimensional spatially resolved spectra, and two-dimensional maps by Integral Field spectroscopy (IFS) of individual galaxies (Cappellari and Copin, 2003; Lu et al., 2023, 2024).

The combined photometric-spectroscopic observations produce maps of galaxy dynamics at high resolution, providing a starting point for comprehensive and accurate probes of galaxy dynamics. Potentially, this brings into view the transition of Newtonian dynamics to anomalous galaxy dynamics further out in galactic disks, that forms the basis of the bTFR. At sufficiently high resolution, these maps may identify a finite sensitivity to aforementioned a_{dS} . Evidence for this sensitivity is found in ensemble-averaged (“stacked”) rotation curves (RC) (van Putten, 2017a,b, 2024b) of SPARC (Lelli et al., 2016; McGaugh et al., 2016). Here, we find a 6σ departure from Λ CDM galaxy models in a sharp C^0 -transition across a_{dS} (van Putten, 2018), distinct from the much smaller scale of acceleration a_0 that parametrizes bTFR of the asymptotic behavior at large radii (Milgrom, 1983; McGaugh, 2012).

Probes of galaxy dynamics in the *Mapping Nearby Galaxies at APO* (MaNGA) survey carry a cumulative uncertainty from instrumental observations, data-processing to stacking, and interpretation with potential contributions from additional sources of data. Already, the intrinsic diversity of individual galaxies introduces noise - intrinsic scatter - with additional contributions from a number of inherent observational challenges (e.g. instrument, atmospheric condition, and reducing raw data and sampling). The

cumulative result defines the total uncertainty budget. In the interpretation of data, further possibly systematic uncertainties may derive from model assumptions, e.g., when involving Mass-to-Light (M/L) ratios based on stellar population synthesis (SPS) and star formation history (SFH) (Conroy, 2013; Zibetti et al., 2009).

In this work, we consider a first step in this direction: the prospect of MaNGA to probing sensitivity to a_{ds} in stacked RCs consistent with the approximately one-percent uncertainty of modern estimates of H_0 . In a necessary but preliminary assessment, we focus on statistical uncertainty - noise from scatter - in sub-samples of varying size N . An unbiased control of N is given by scatter in-the-mean σ/\sqrt{N} in the three Position Angles (PAs) obtained from photometric images and gas and stellar velocity fields. In a regular propagation of uncertainty (below), σ/\sqrt{N} is expected to set a minimum to the total uncertainty budget in stacked RCs. Aiming to probe galaxy dynamics at uncertainties on par with observations of H_0 , we set out to determine that MaNGA is sufficiently large to allow σ/\sqrt{N} to reach about one percent.

MaNGA data release 17 (Bundy et al., 2015) covers the largest number of galaxies with IFU observations to date. For any ensemble-averaged observable, the scatter σ in the three PAs of photometric images and the velocity fields of gas and stars by spectroscopy conceivably defines a significant contribution to the standard error in the mean S_E . More generally, we have (e.g. Ku, 1966; Hibat-Allah et al., 2023; Stone et al., 2021)

$$S_E = \frac{\sqrt{\kappa^2\sigma^2 + \dots}}{\sqrt{N}} \quad (2)$$

for a sample size N , where κ is a constant of order unity assuming regular propagation of uncertainty - the scatter in-the-mean σ/\sqrt{N} - and the dots refer to contributions from additional and statistically independent sources of noise in the data. To exemplify, of particular interest is the accurate measurement of the bTFR (McGaugh, 2012) and, deeper within galaxies, the location a_{ds} of the C^0 -transition of Newtonian to anomalous gravitation - in SPARC (van Putten, 2018), awaiting confirmation in an independent survey such as MaNGA.

In §2, we present our MaNGA sample selection of spiral galaxies. In §3, we present our unbiased parameter controlling the size $N = N_i(\theta)$ of sub-samples by bounding consistency θ in the three PAs in MaNGA, binned over various inclination angles i . Scatter in-the-mean σ/\sqrt{N} in (2) as a function of θ is presented in §3, showing the desired control down to about one percent. In §4, we discuss an outlook on probing sensitivity of galaxy dynamics to a_{ds} in stacked MaNGA RCs and its applications to cosmological parameter estimation.

2. Selection of MaNGA spiral galaxies

MaNGA is a part of the Fourth-Generation *Sloan Digital Sky Survey* (SDSS-IV, (Blanton et al., 2017)). It provides spatially resolved spectral measurements of about 10,000 galaxies. The primary sample provides radial coverage over approximately 1.5 half-light radii (R_e), included in 67% of MaNGA. The secondary sample extends radial coverage to 2.5 R_e , included in the remaining 33%. The optical wavelengths of BOSS Spectrographs in MaNGA span $0.36\mu\lesssim\lambda\lesssim1.0\mu$ with a resolution $R \sim 2000$ (Westfall et al., 2019). The mean redshift of MaNGA galaxies is approximately 0.03 with a roughly flat stellar mass distribution, $M_* \gtrsim 10^9 M_\odot$.

The MaNGA data release includes almost every level of data reduction. Starting from raw data, a comprehensive 3-D data reduction pipeline (DRP) extends to a data-analysis pipeline(DAP). DRP output is flatfield-subtracted, sky-subtracted, position-calibrated, flux-calibrated, sampled to a common wavelength grid, and so on. DAP provides DRP assessments, spatial binning, stellar-continuum modeling, emission-line measurements, spectral measurement and more (Westfall et al., 2019).

DAP includes three different binning schemes in DAP output:

- Individual spaxel binning (SPX);
- Spaxel binning with $S/N \sim 10$ by Voronoi (VOR10) (Cappellari and Copin, 2003);
- Same as VOR10 binning to stellar continuum analysis for stellar kinematics, and individual binning for emission-line measurements (HYB10).

In stellar continuum analysis providing stellar kinematics, hierarchically clustered MILES templates are used (MILESHC) for all the data. In continuum+emission-line modeling, DAP includes two types: simple stellar population models (MASTARSSP) derived from MaStar (MaNGA Stellar Library (Yan et al., 2019)) and hierarchically clustered templates (MASTARHC2) from MaStar. With the above-mentioned schemes, four DAPTYPE of data are provided. Among these, we select the DAP output HYB10-MILESHC-MASTARSSP combination, as HYB10 data is expected to provide the best spatial resolution for emission-line analysis.

Focusing on galaxy rotation curves, we select the MaNGA *Deep Learning Morphology Value Added Catalog* (MDLM-VAC-DR17) to select late-type galaxies (Domínguez Sánchez et al., 2022). This catalog provides deep-learning-based morphological classification for MaNGA samples. MDLM-VAC-DR17 used SDSS-DR7 RGB-cutout as input and trained a convolutional neural

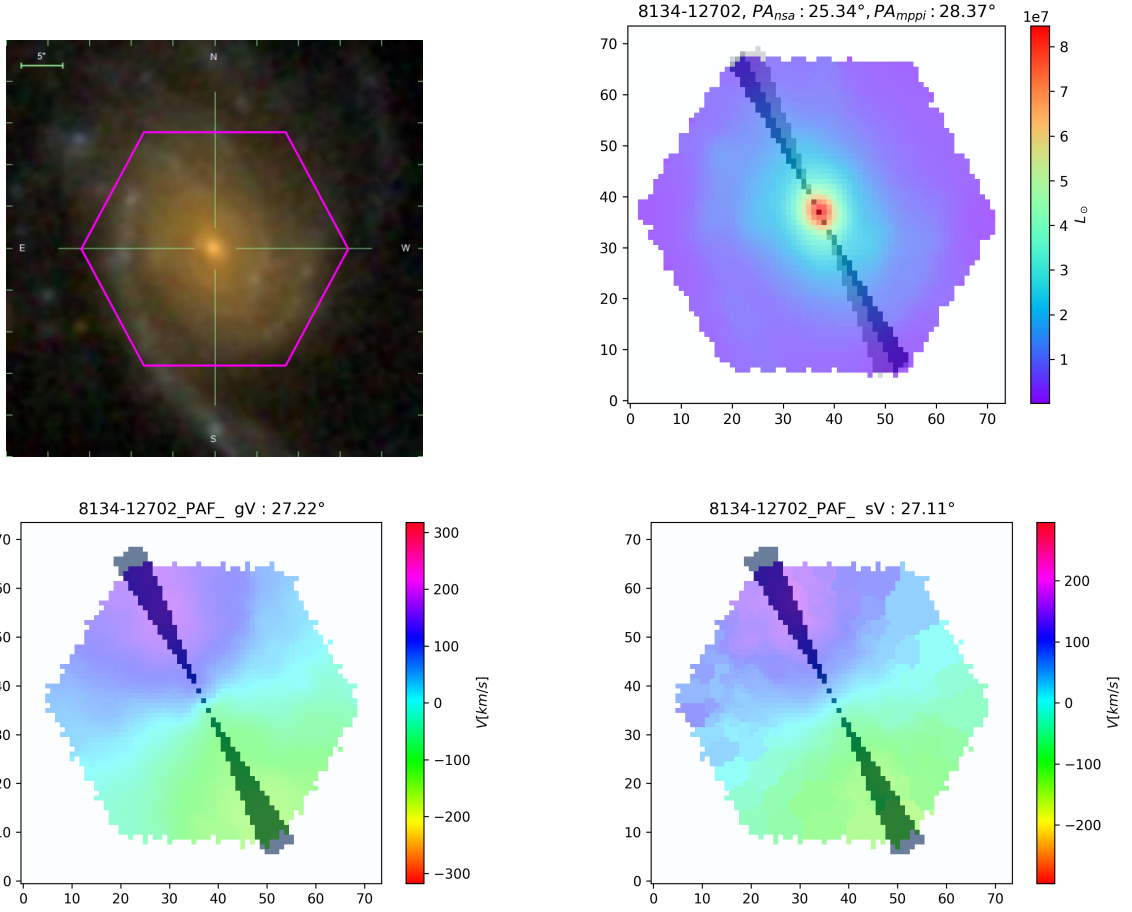


Figure 1: Photometric and spectroscopic data of a MaNGA galaxy, 8134-12702 MaNGA galaxy 8134-12702. Top left: SDSS photometric image. Top right: MaNGA i-band image overplotted with position angles from NSA catalog and MPP VAC with $PA_{ph} = 25.34^\circ$ and $PA_{ph} = 28.37^\circ$ respectively. Bottom : Gas velocity map and stellar velocity map from right to the left respectively with small-angle pencil beams (grey shade) show $PA_g = 27.22^\circ$ and $PA_s = 27.11^\circ$ in least-squares sine-fits to the velocity field over an opening angle of 12° .

network (CNN) with this input for each classification task. Further detailed methodology is provided in (Domínguez Sánchez et al., 2018).

In the MDLM-VAC-DR17 classification, positive T-Type corresponds to late-type galaxies (LTGs), and negative T-Type corresponds to early-type galaxies (ETGs). According to T-Type, galaxies are subdivided into sub-classes through additional training (CNN) when needed. Following the above, MDLM-VAC-DR17 provides P_LTG, P_S0, P_edge-on, P_bar, representing the respective probabilities. T-Type and P_S0 combined present the three broad categories E, S0, and S. It includes a sub-division for S galaxies into S1 and S2 according to the T-Type. After visual inspection, they report the result in Visual Class (VC = 1,2,3, and 0 for E, S0, S/Irr and unclassifiable, respectively), and Visual Flag (VF=0 for reliable and 1 for uncertain). Our initial selection of MaNGA sample contains 5125 galaxies according to $P_{LTG} > 0.5$, positive T-Type, VC = 3 and VF = 0, recommended for spiral galaxies in MDLM-VAC-DR17.

We downselect according to the MaNGA DAP quality flag *bitmask*, removing 713 galaxies satisfying either of the following: (1) identified foreground stars, (2) NSA (NASA-Sloan Atlas) redshift inconsistency, (3) no emission line, (4) ppxf fit failure, (5) Voronoi binning failure, (6) invalid input geometry, (7) critical failure in DRP, (8) critical failure in DAP, or (9) critical failure in DRP or DAP. Table 1 shows the remaining sample of $N = 4412$ galaxies. Table 1 is the starting point of our analysis, differentiating our sample in bins of inclination angle i by 10° intervals. The inclination angles i of the galaxies are calculated from axis-ratios b/a , evaluated at 90% light-radius provided by NASA-Sloan Atlas (NSA) catalog. We next downloaded above-mentioned DAPTYPE data 'HYB10-MILESHC-MASTARSSP' and 'HYB10-MILESHC-MASTARHC2' from MaNGA for our sample of $N = 4412$ galaxies, except for one (MaNGA Plate-IFU 8626-9102, in the bin $50^\circ - 60^\circ$) that appears unavailable from the MaNGA server. This leaves a total count of our MaNGA spiral galaxy selection of $N = 4411$.

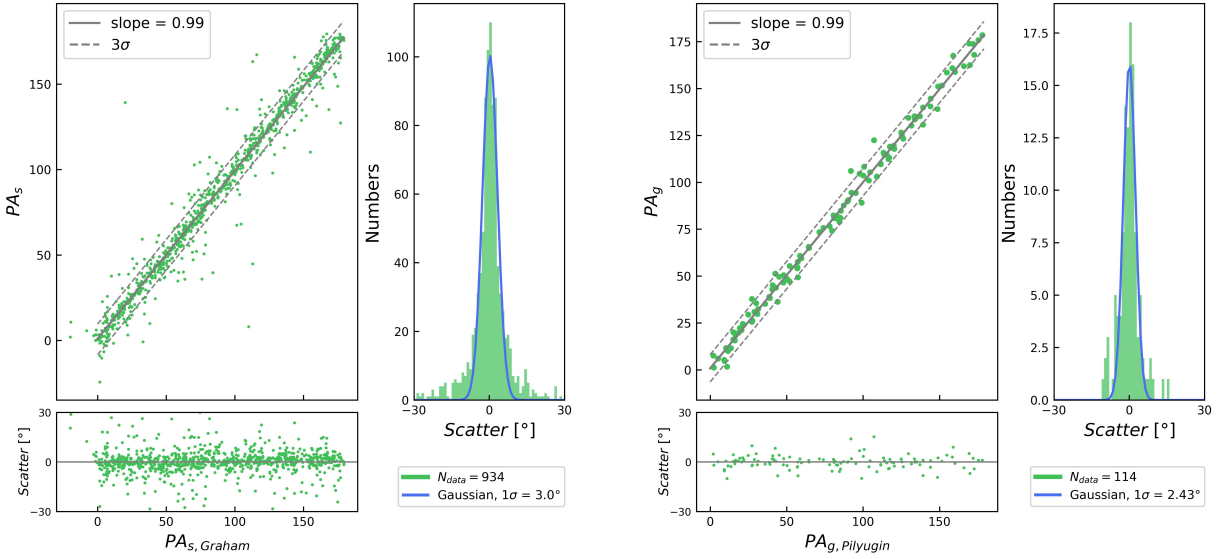


Figure 2: (Left panels.) Cross-check of our PA_s with $PA_{s,Graham}$ from Graham et al. (2018), for 934 galaxies in our sample (Table 1) in common with those of a MaNGA subset of 2721 galaxies in (Graham et al., 2018). (Right panels.) Cross-check of our PA_g with $PA_{g,Pilyugin}$ from Pilyugin et al. (2019), for 114 galaxies in our sample (Table 1) in common with among the sample of Pilyugin et al. (2019).

3. Statistics of consistency in Position Angles

In a high-resolution analysis of ensemble-averaged data, statistical uncertainty is governed by errors in-the-mean controlled by sample size N for a given scatter σ in the data. This consideration does not include systematic errors, that typically is case-specific. In regular propagation of uncertainties, contributions to a standard error in-the-mean S_E satisfy canonical scaling with σ/\sqrt{N} , the constant of proportionality κ highlighted in (2) generally depending on the choice of observable. For our MaNGA sub-sample of spiral galaxies (§2), we expect a potentially significant contribution from scatter in the three PAs of photometry and the velocity fields of gas and stars from spectroscopy, assuming regular propagation of uncertainty quantified by κ in (2). A full account of this contribution to the total noise budget requires measuring κ in (2) by varying the control parameter θ , separate from other (statistically independent) sources of noise in the data. To this end, we proceed as follows.

Consistency of the PAs in the velocity fields of gas and stars is defined by the difference

$$\Delta_1 PA = PA_g - PA_s. \quad (3)$$

Fig. 1 shows an example of velocity fields of gas and stars. We analyze these data in a polar coordinate system (r, φ) with its origin at the galaxy center provided by MaNGA. Using best-fit by the least-squares method, we derive the $PA = \varphi_0 + \pi/2$ according to the maximum of the amplitudes $A = A(r)$ in fits $A \sin(\varphi - \varphi_0) + b$ over all $0 \leq \varphi \leq 2\pi$ for given $r \geq 0$, where b refers to an ignorable velocity offset. This procedure is repeated twice with an initial guess of PA based on photometric images in the NSA catalogue. We confirmed that our results are rather insensitive to uncertainty in inclination angles i following various injection experiments. As shown in Fig. 1, we use a 12° width of a PA in scans over φ over increments of 1° . Results are found to be robust against choice of this angular width.

In using various photometric parameters including bulge parameters, we choose to use the MaNGA *PyMorph Photometric Value Added Catalog* (MPP VAC). To probe PA consistency, we downselect samples successfully allowing for a one-component Sersic-fit (in MPP VAC). These samples can be presented with one PA extending over the entire galaxy radius, while others are failed to have one-component Sersic-fit partly because of bulges and/or bars structures, or other unknown reasons.

This downselection leaves $N = 4067$ spiral galaxies. Focused furthermore on the MaNGA *Principal Component Analysis Value Added Catalog* (PCA VAC), leaves a total of $N = 4053$ spiral galaxies.

As a cross-check, Fig. 2 shows two comparisons of our PAs with PAs from the literature. 114 galaxies are in common with samples from Pilyugin et al. (2019) which provides 147 MaNGA galaxy properties including PAs obtained by gas velocity fields. From Graham et al. (2018) providing PAs obtained from stellar velocity fields, we cross-checked 934 galaxy PAs of stellar velocity fields.

Fig. 3 shows the resulting 2D distributions of ΔPA obtained from velocity fields (horizontal axis) and photometry (vertical axis)

following (3) and, respectively,

$$\Delta_2 \text{PA} = \text{PA}_{ph} - \text{PA}_{vf} \quad (4)$$

between PA_{ph} of photometry and the mean

$$\text{PA}_{vf} = \frac{1}{2} (\text{PA}_g + \text{PA}_s). \quad (5)$$

Fig. 3 is restricted to consistency within 30° , containing a remainder of $N = 3101$ galaxies detailed in Column 9 of Table 1.

The two traces $\Delta_k \text{PA}$, $k = 1, 2$, of the 2D distribution of ΔPA can be suitably fitted by Gaussian distributions (side-panels in Fig. 3). The standard deviations σ_G of these Gaussian fits tend to be smaller than the standard deviations of the data (Table 2). This indicates that the tails of our distributions are non-Gaussian. It is further noted that this discrepancy in standard deviation appears mostly at relatively small inclination angles and more so in $\Delta_1 \text{PA}$ than in $\Delta_2 \text{PA}$, even though the latter shows more noise than the former.

We are at liberty to select sub-samples from the 2D distribution of Fig. 3 according to the strips

$$|\Delta_k \text{PA}| < \theta \quad (6)$$

over $0 < \theta < 30^\circ$, where $k = 1, 2$. In considering (6) for $\Delta_1 \text{PA}$, $\Delta_2 \text{PA}$ is left unbounded and vice versa. Table 2 lists the sizes N_i and associated standard deviations, derived from the 2D distribution of Fig. 3, further differentiated over a range of inclination angles i .

Table 1: Standard deviations in the 2D distribution of PA angle differences $\Delta_1 \text{PA}$, $\Delta_2 \text{PA}$, and $\Delta_b \text{PA}$ of Fig. 3, listed by bin of inclination i .

i	All			$ \Delta_1 \text{PA} < 30^\circ$		$ \Delta_2 \text{PA} < 30^\circ$		$ \Delta_b \text{PA} < 30^\circ$		
	N_i	$\sigma_{(i, \Delta_1 \text{PA})}$	$\sigma_{(i, \Delta_2 \text{PA})}$	N_i	$\sigma_{(i, \Delta_1 \text{PA})}$	N_i	$\sigma_{(i, \Delta_2 \text{PA})}$	N_i	$\sigma_{(i, \Delta_1 \text{PA})}$	$\sigma_{(i, \Delta_2 \text{PA})}$
$i < 30^\circ$	337	20.1°	42.85°	301 (89%)	9.64°	187(55%)	15.24°	172 (51%)	8.67°	14.68°
$30^\circ \leq i < 40^\circ$	392	21.1°	35.46°	341(87%)	9.04°	255(65%)	13.01°	237(60%)	7.25°	12.67°
$40^\circ \leq i < 50^\circ$	559	19.67°	32.48°	506(91%)	9.57°	414(74%)	11.65°	393(70%)	8.56°	11.34°
$50^\circ \leq i < 60^\circ$	674	17.53°	27.61°	621(92%)	8.94°	550(82%)	11.62°	524(78%)	8.27°	11.42°
$60^\circ \leq i < 70^\circ$	761	20.23°	23.39°	685(99%)	9.65°	666(88%)	9.79°	635(83%)	9.17°	9.02°
$70^\circ \leq i < 80^\circ$	753	20.01°	23.09°	679(98%)	8.99°	672(89%)	8.14°	636(84%)	8.31°	7.03°
$i \geq 80^\circ$	577	17.62°	19.67°	532 (96%)	7.79°	526(91%)	7.52°	505(88%)	7.38°	6.78°

The large- N MaNGA sample allows detailed control of σ/\sqrt{N} upon selecting sub-samples over strips (6) from the 2D distribution of Fig. 3. For a given ensemble-averaged observable, contributions to a standard error in-the-mean (2) can hereby be explicitly evaluated according to

$$\kappa_k = \frac{\partial S_E}{\partial (\sigma/\sqrt{N})_k}, \quad (7)$$

where $k = 1, 2$. To quantify this, Fig. 4 shows the scatter in-the-mean, σ/\sqrt{N} with respect to our control parameter θ in (6). The black curves in Fig. 4 represent our results in the mean over $i < 80^\circ$ with quadratic fits over $0 < \theta < 30^\circ$ satisfying

$$\begin{aligned} \left(\frac{\sigma}{\sqrt{N}}\right)_1 &\simeq 0.104 + 0.038 \theta - 5.3 \times 10^{-4} \theta^2, \\ \left(\frac{\sigma}{\sqrt{N}}\right)_2 &\simeq 0.244 + 0.041 \theta - 2.4 \times 10^{-4} \theta^2. \end{aligned} \quad (8)$$

We next consider sub-samples within the box defined by the intersection of the two strips (6). Within this box,

$$|\Delta_b \text{PA}| < \theta, \quad (9)$$

scatter is bounded by θ simultaneously for both $\Delta_1 \text{PA}$ and $\Delta_2 \text{PA}$. Table 2 shows $\Delta_1 \text{PA}$ and $\Delta_2 \text{PA}$ to be essentially uncorrelated by their small Pearson coefficients. Accordingly, we have $\sigma_b \simeq \sqrt{\sigma_1^2 + \sigma_2^2}$. A linear fit to the scatter in the mean over (9) over $\theta < 30^\circ$ (Fig. 4) satisfies

$$\left(\frac{\sigma}{\sqrt{N}}\right)_b \simeq (0.625 + 0.031 \theta^\circ)[\% \text{rad}]. \quad (10)$$

This relation shows control of scatter in PA differences by choice of $0 < \theta \leq 30^\circ$. In particular, scatter is a mere 1.6 % rad at $\theta = 30^\circ$, reducing to 0.94 % rad at $\theta = 10^\circ$. These values set one-percent lower bounds on a total standard error in-the-mean S_E in ensemble averages. In practice, S_E will be larger upon including additional data beyond and independent of the present PAs.

Summarized in Fig. 4 and (10), our results on scatter in three PAs demonstrates the potential of MaNGA for high-resolution studies in ensemble-averaged observables of galaxy dynamics on par with modern precision cosmology.

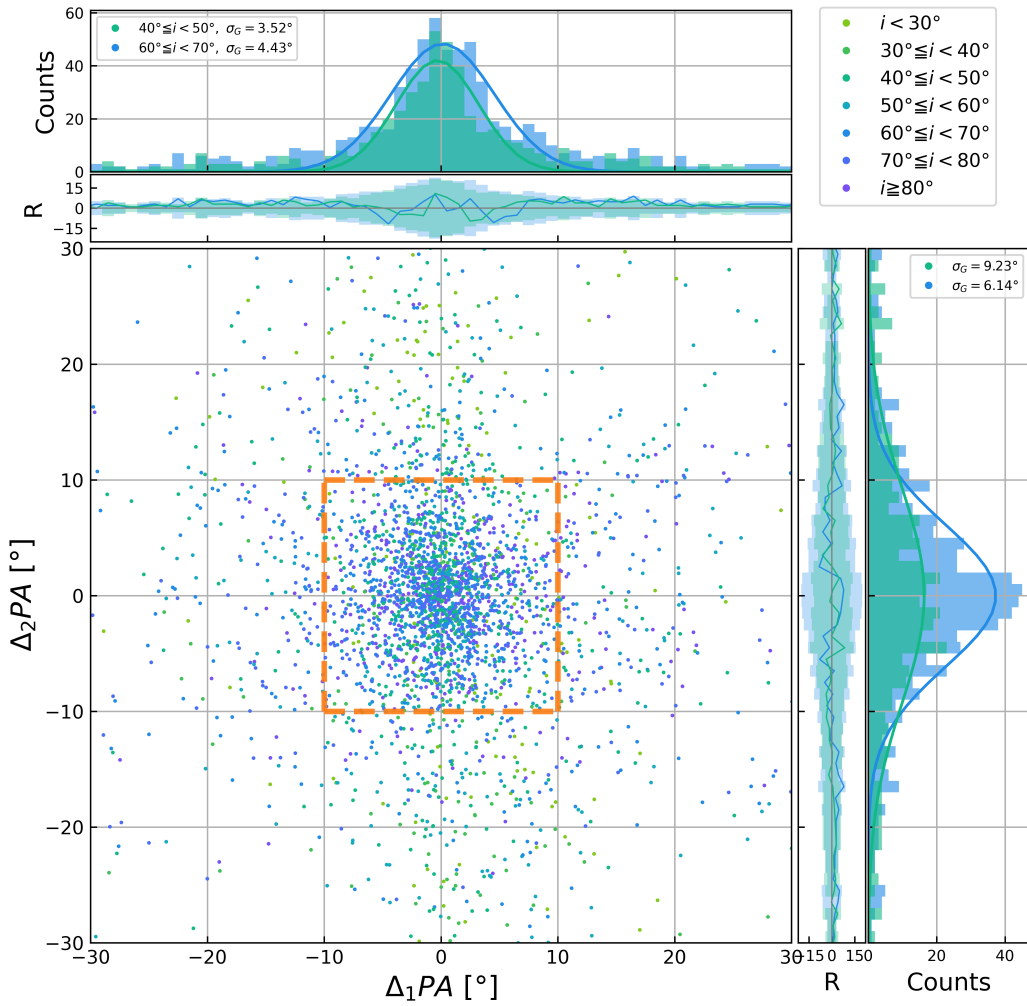


Figure 3: The 2D-distribution of $\Delta_1 PA$ in (3) in the velocity fields of gas and stars (horizontal axis) and $\Delta_2 PA$ in (4) between the PA in photometry and the mean of the two PAs in velocity fields (vertical axis). The distribution is largely Gaussian within $\pm 30^\circ$ except for some excess in tails. The top and rightmost plot shows the number distributions versus the control parameter θ according to (3) and (4), further showing the accompanying Gaussian fits and 3σ uncertainties by scatter in Poisson noise. The dashed orange square indicates a choice of box of $|\Delta_b PA| < \theta$ (9), shown for $\theta = 10^\circ$, bounding both $\Delta_1 PA$ and $\Delta_2 PA$.

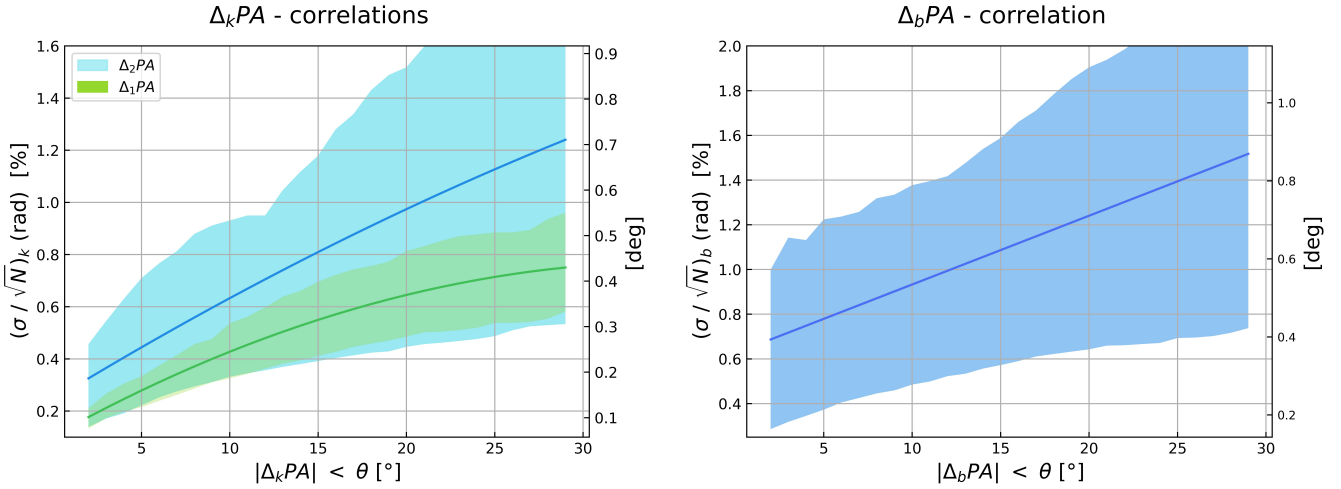


Figure 4: Overview of scatter in-the-mean σ / \sqrt{N} of the three PAs in MaNGA over $i < 80^\circ$ based on Table 2, excluding anomalous results for $i \geq 80^\circ$. Scatter is defined according to the differences $|\Delta_k PA| < \theta$ ($k = 1, 2$) among the three PAs of the photometric image and velocity fields. The black solid lines are fitted line in quadratic formula for left panel, and in linear for right panel. The fit coefficients are provided in (8). (Left panel.) Scatter as a function of the control parameter θ . While small, PAs of the velocity fields of gas and stars are noticeably more consistent than the same relative to the PA derived from photometry. (Right panel.) Scatter within the two-dimensional box $|\Delta_b PA| < \theta$ restricting both $\Delta_1 PA$ and $\Delta_2 PA$ simultaneously. The results evidence consistency in MaNGRA sub-samples measured by PAs down to about one percent, providing a suitable starting point for accurate probes of ensemble-averaged rotation curves. The contribution to the total noise budget of σ / \sqrt{N} in (2) derives from κ , determined by varying the control parameter θ .

Table 2: Pearson coefficients r_{12} of $\Delta_1 PA$ and $\Delta_2 PA$ of Fig. 3, listed by bin of inclination angle i . Results indicate statistical independence of $\Delta_1 PA$ and $\Delta_2 PA$ within the expected statistical uncertainty $1 / \sqrt{N_i}$ of the Pearson coefficient of size N_i drawn from normal distributions. The last three columns refer to the Pearson coefficients r_{12} of $\Delta_1 PA$ and $\Delta_2 PA$ within the strips (6) of maximal width $\theta = 30^\circ$. For the corresponding box of maximal size, correlations remain small on average, though with finite correlations slightly away from zero (last column).

Inclination i	N_i	r_{12}	$r_{12} \sqrt{N_i}$	$N_i(\Delta_b PA < 30^\circ)$	$r_{12}(\Delta_b PA < 30^\circ)$	$r_{12} \sqrt{N_i}(\Delta_b PA < 30^\circ)$
$i < 30^\circ$	337	-0.058	-1.0647	172	0.1971	2.5849
$30^\circ \leq i < 40^\circ$	392	0.0306	0.6058	237	0.0791	1.2177
$40^\circ \leq i < 50^\circ$	559	0.0291	0.688	393	0.0682	1.352
$50^\circ \leq i < 60^\circ$	674	-0.003	-0.0779	523	0.112	0.4528
$60^\circ \leq i < 70^\circ$	761	0.0758	2.091	635	0.1137	2.8223
$70^\circ \leq i < 80^\circ$	753	0.0314	0.8616	636	-0.0106	-0.2673
$i \geq 80^\circ$	577	0.1128	2.7095	505	-0.0041	-0.0921

4. Outlook

Probing sensitivity of galaxy dynamics at a level of (statistical) uncertainty on par with modern cosmological parameters is a major objective to advancing our understanding of weak gravitation, potentially across all redshifts upon including recent results of JWST. While Λ CDM assumes Newtonian gravitation to be scale-free and valid down to arbitrarily small accelerations, conceivably weak gravity in RCs and gravitational collapse producing the first galaxies at cosmic dawn is subject to the background de Sitter scale a_{ds} . If so, this offers a prospect of unifying the bTFR and the JWST ‘Impossible galaxies’ (van Putten, 2024b).

Fig. 4 summarizes our main finding: MaNGA provides the required large N to control scatter in-the-mean of three PAs of photometric images and spectroscopic velocity fields down to the one-percent level. As a minimum to the total uncertainty budget (2), this offers a prospect for high-resolution analysis of stacked MaNGA RCs, provided that the present scatter in PAs provides an effective proxy for any additional sources of noise and uncertainty.

In particular, we seek to control scatter in-the-mean in ensemble-averaged rotation curves to accurately resolve the transition to accelerations below a_{ds} . In coordinate space, this occurs at the transition radius (van Putten, 2017a)

$$r_t = \sqrt{R_G R_H} \simeq 4.7 \text{ kpc } M_{11}^{1/2}, \quad (11)$$

where $R_G = GM_b/c^2$ is the gravitational radius of a galaxy of baryonic mass $M_b = M_{11} 10^{11} M_\odot$ and $R_H = c/H$ is the Hubble radius, given a Hubble parameter $H = H_0$ at the present epoch. For the Milky Way and similar galaxies, therefore, most of the disk is at accelerations $\alpha < a_{ds}$. To confirm previous results, we aim for improved resolution and rigor with MaNGA as an independent and

much larger catalog than SPARC. Stacking of normalized RCs is envisioned in the plane of a_N/α versus a_N/a_{ds} , where a_N is the expected Newtonian acceleration based on Newton's law of gravitation and baryonic mass content and $\alpha = V_c^2/r$ is the centripetal acceleration derived from the presented photometric-spectroscopic data.

By virtue of the large- N MaNGA survey and statistical independence of PAs (Table 3), contributions of Δ_1 PA and Δ_2 PA in (2) can be individually identified by their respective κ values (7). We can also consider their joint contribution, considering sub-samples in the box $|\Delta_b\text{PA}| < \theta$, bounding scatter jointly in the $\Delta_1\text{PA}$ and $\Delta_2\text{PA}$ with the same θ . The resulting scatter in-the-mean is about one percent with modest dependence on θ (Fig. 4).

Conceivably, scatter in the PAs can be reduced by galaxy modeling, e.g., Pilyugin et al. (2020); Warner et al. (1973); Begeman (1989); de Blok et al. (2008); Oh et al. (2018); Pilyugin et al. (2019); Oh et al. (2018). Fig. 4, however, shows our present estimates already to satisfy our one percent criterion.

While scatter in PAs is not the only source of noise, we expect it to be a significant contributor to the total noise budget of any observable of ensemble-averaged rotation curves in (2). Crucially, large sub-samples of MaNGA can be selected within a bound $(|\theta| < 30^\circ)$ (Table 2). Their sizes $N_i(\theta)$ remain sufficiently large to permit a detailed measurement of the coefficient κ in (2) for each bin of inclination angles i at uncertainties on the order of a few percent by varying the control parameter θ .

Accordingly, MaNGA promises just the kind of large- N survey permitting a high-resolution probe of sensitivity to background cosmology. Our focal point is the transition (11) of Newtonian to anomalous gravitation in galaxy dynamics across a_{ds} , marked by what appears to be a C^0 -transition in normalized galaxy RCs. At the intended one-percent level of scatter in-the-mean, resolving a_{ds} and hence H_0 may be used to distinguish between *Planck* Λ CDM and LDL in light of the H_0 -tension of about 9% between the two (van Putten, 2021; Riess et al., 2022). Importantly, a_{ds} and the much smaller scale a_0 are related (van Putten, 2024a)

$$a_0 = \frac{c^2}{2\pi} \sqrt{J}. \quad (12)$$

Here, $J = (1 - q) H^2/c^2$ is the trace of the Schouten tensor (van Putten, 2024b, 2025) and q denotes the deceleration parameter of the background cosmology. This relationship elucidates redshift dependence in a_0 specific to the cosmological background. Indeed, with H_0 at hand, (12) can be used to estimate q_0 , even though, at present, with very large uncertainty (van Putten, 2024b).

The present results suggest that MaNGA can provide a confirmation of a_{ds} in the transition to anomalous galaxy dynamics, independent of SPARC, which asymptotes to the bTFR parameterized by a_0 . According to our results, stacked MaNGA RCs appear promising to accurately resolve these two distinct scales of acceleration a_{ds} and a_0 governing weak gravitation in galaxy dynamics, further across a small but finite range of cosmological redshift.

CRediT authorship contribution statement

G.-M. Lee: Writing, Investigation, Visualization, Formal analysis, Data curation, Validation, Software. **M.H.P.M. van Putten:** Conceptualization, Writing — original draft, review & editing, Validation, Funding acquisition, Supervision.

Declaration of competing interest

The authors declare that they have no known competing financial interests or personal relationships that could have appeared to influence the work reported in this paper.

Acknowledgments

The authors thank the anonymous reviewer for a detailed reading and constructive comments. This work was supported, in part, by NRF grant No. RS-2024-00334550.

Data Availability

The data underlying this article are available in the MaNGA archives through the MaNGA online data base.

References

- Begeman, K.G., 1989. HI rotation curves of spiral galaxies. I. NGC 3198. *A&A* 223, 47–60.
 Bell, E.F., de Jong, R.S., 2001. Stellar Mass-to-Light Ratios and the Tully-Fisher Relation. *ApJ* 550, 212–229. doi:10.1086/319728, arXiv:astro-ph/0011493.
 Blanton, M.R., Bershadsky, M.A., Abolfathi, B., Albareti, F.D., Allende Prieto, C., Almeida, A., Alonso-García, J., Anders, F., Anderson, S.F., Andrews, B., Aquino-Ortíz, E., Aragón-Salamanca, A., Argudo-Fernández, M., Armengaud, E., Aubourg, E., Avila-Reese, V., Badenes, C., Bailey, S., Barger, K.A., Barrera-Ballesteros, J., Bartosz, C., Bates, D., Baumgarten, F., Bautista, J., Beaton, R., Beers, T.C., Belfiore, F., Bender, C.F., Berlind, A.A., Bernardi, M., Beutler, F., Bird, J.C., Bizyaev, D., Blanc, G.A., Blomqvist, M., Bolton, A.S., Boquien, M., Borissova, J., van den Bosch, R., Bovy, J., Brandt, W.N., Brinkmann, J., Brownstein, J.R., Bundy, K., Burgasser, A.J., Burtin, E., Busca, N.G., Cappellari, M., Delgado Carigi, M.L., Carlberg, J.K., Carnero Rosell, A., Carrera, R.,

- Chanover, N.J., Cherinka, B., Cheung, E., Gómez Maqueo Chew, Y., Chiappini, C., Choi, P.D., Chojnowski, D., Chuang, C.H., Chung, H., Cirolini, R.F., Clerc, N., Cohen, R.E., Comparat, J., da Costa, L., Cousinou, M.C., Covey, K., Crane, J.D., Croft, R.A.C., Cruz-Gonzalez, I., Garrido Cuadra, D., Cunha, K., Damke, G.J., Darling, J., Davies, R., Dawson, K., de la Macorra, A., Dell'Agli, F., De Lee, N., Delubac, T., Di Mille, F., Diamond-Stanic, A., Cano-Díaz, M., Donor, J., Downes, J.J., Drory, N., du Mas des Bourboux, H., Duckworth, C.J., Dwelly, T., Dyer, J., Ebelke, G., Eigenbrot, A.D., Eisenstein, D.J., Emsellem, E., Eracleous, M., Escoffier, S., Evans, M.L., Fan, X., Fernández-Alvar, E., Fernandez-Trincado, J.G., Feuillet, D.K., Finoguenov, A., Fleming, S.W., Font-Ribera, A., Fredrickson, A., Freischlad, G., Frinchaboy, P.M., Fuentes, C.E., Galbany, L., García-Díaz, R., García-Hernández, D.A., Gaulme, P., Geisler, D., Gelfand, J.D., Gil-Marín, H., Gillespie, B.A., Goddard, D., Gonzalez-Perez, V., Grabowski, K., Green, P.J., Grier, C.J., Gunn, J.E., Guo, H., Guy, J., Hagen, A., Hahn, C., Hall, M., Harding, P., Hasselquist, S., Hawley, S.L., Hearty, F., Gonzalez Hernández, J.I., Ho, S., Hogg, D.W., Holley-Bockelmann, K., Holtzman, J.A., Holzer, P.H., Huehnerhoff, J., Hutchinson, T.A., Hwang, H.S., Ibarra-Medel, H.J., da Silva Ilha, G., Ivans, I.I., Ivory, K., Jackson, K., Jensen, T.W., Johnson, J.A., Jones, A., Jönsson, H., Jullo, E., Kamble, V., Kinemuchi, K., Kirkby, D., Kitaura, F.S., Klaene, M., Knapp, G.R., Kneib, J.P., Kollmeier, J.A., Lacerna, I., Lane, R.R., Lang, D., Law, D.R., Lazarz, D., Lee, Y., Le Goff, J.M., Liang, F.H., Li, C., Li, H., Lian, J., Lima, M., Lin, L., Lin, Y.T., Bertran de Lis, S., Liu, C., de Icaza Lizaola, M.A.C., Long, D., Lucatello, S., Lundgren, B., MacDonald, N.K., Deconto Machado, A., MacLeod, C.L., Mahadevan, S., Geimba Maia, M.A., Maiolino, R., Majewski, S.R., Malanushenko, E., Malanushenko, V., Manchado, A., Mao, S., Maraston, C., Marques-Chaves, R., Masseron, T., Masters, K.L., McBride, C.K., McDermid, R.M., McGrath, B., McGreer, I.D., Medina Peña, N., Melendez, M., Merloni, A., Merrifield, M.R., Meszaros, S., Meza, A., Minchev, I., Minniti, D., Miyaji, T., More, S., Mulchaey, J., Müller-Sánchez, F., Munoz, D., Munoz, R.R., Myers, A.D., Nair, P., Nandra, K., Correa do Nascimento, J., Negrete, A., Ness, M., Newman, J.A., Nichol, R.C., Nidever, D.L., Nitschelm, C., Ntelis, P., O'Connell, J.E., Oelkers, R.J., Oravetz, A., Oravetz, D., Pace, Z., Padilla, N., Palanque-Delabrouille, N., Alonso Palicio, P., Pan, K., Parejko, J.K., Parikh, T., Páris, I., Park, C., Patten, A.Y., Peirani, S., Pellejero-Ibanez, M., Penny, S., Percival, W.J., Perez-Fournon, I., Petitjean, P., Pieri, M.M., Pinsonneault, M., Pisani, A., Poleski, R., Prada, F., Prakash, A., Queiroz, A.B.d.A., Raddick, M.J., Raichoor, A., Barboza Rembold, S., Richstein, H., Riffel, R.A., Riffel, R., Rix, H.W., Robin, A.C., Rockosi, C.M., Rodríguez-Torres, S., Roman-Lopes, A., Román-Zúñiga, C., Rosado, M., Ross, A.J., Rossi, G., Ruan, J., Ruggeri, R., Rykoff, E.S., Salazar-Albornoz, S., Salvato, M., Sánchez, A.G., Aguado, D.S., Sánchez-Gallego, J.R., Santana, F.A., Santiago, B.X., Sayres, C., Schiavon, R.P., da Silva Schimoia, J., Schlafly, E.F., Schlegel, D.J., Schneider, D.P., Schultheis, M., Schuster, W.J., Schwone, A., Seo, H.J., Shao, Z., Shen, S., Shetrone, M., Shull, M., Simon, J.D., Skinner, D., Skrutskie, M.F., Slosar, A., Smith, V.V., Sobbeck, J.S., Sobreira, F., Somers, G., Souto, D., Stark, D.V., Stassun, K., Stauffer, F., Steinmetz, M., Storchi-Bergmann, T., Streblyanska, A., Stringfellow, G.S., Suárez, G., Sun, J., Suzuki, N., Szegedi, L., Taghizadeh-Popp, M., Tang, B., Tao, C., Tayar, J., Tembe, M., Teske, J., Thakar, A.R., Thomas, D., Thompson, B.A., Tinker, J.L., Tissera, P., Tojeiro, R., Hernandez Toledo, H., de la Torre, S., Tremonti, C., Troup, N.W., Valenzuela, O., Martinez Valpuesta, I., Vargas-González, J., Vargas-Magaña, M., Vazquez, J.A., Villanova, S., Vivek, M., Vogt, N., Wake, D., Walterbos, R., Wang, Y., Weaver, B.A., Weijmans, A.M., Weinberg, D.H., Westfall, K.B., Whelan, D.G., Wild, V., Wilson, J., Wood-Vasey, W.M., Wylezalek, D., Xiao, T., Yan, R., Yang, M., Ybarra, J.E., Yéche, C., Zakamska, N., Zamora, O., Zarrouk, P., Zasowski, G., Zhang, K., Zhao, G.B., Zheng, Z., Zheng, Z., Zhou, X., Zhou, Z.M., Zhu, G.B., Zoccali, M., Zou, H., 2017. Sloan Digital Sky Survey IV: Mapping the Milky Way, Nearby Galaxies, and the Distant Universe. *AJ* 154, 28. doi:10.3847/1538-3881/aa7567, arXiv:1703.00052.
- Brinchmann, J., Charlot, S., White, S.D.M., Tremonti, C., Kauffmann, G., Heckman, T., Brinkmann, J., 2004. The physical properties of star-forming galaxies in the low-redshift Universe. *MNRAS* 351, 1151–1179. doi:10.1111/j.1365-2966.2004.07881.x, arXiv:astro-ph/0311060.
- Bundy, K., Bershadsky, M.A., Law, D.R., Yan, R., Drory, N., MacDonald, N., Wake, D.A., Cherinka, B., Sánchez-Gallego, J.R., Weijmans, A.M., Thomas, D., Tremonti, C., Masters, K., Coccato, L., Diamond-Stanic, A.M., Aragón-Salamanca, A., Avila-Reese, V., Badenes, C., Falcón-Barroso, J., Belfiore, F., Bizyaev, D., Blanc, G.A., Bland-Hawthorn, J., Blanton, M.R., Brownstein, J.R., Byler, N., Cappellari, M., Conroy, C., Dutton, A.A., Emsellem, E., Etherington, J., Frinchaboy, P.M., Fu, H., Gunn, J.E., Harding, P., Johnston, E.J., Kauffmann, G., Kinemuchi, K., Klaene, M.A., Knapen, J.H., Leauthaud, A., Li, C., Lin, L., Maiolino, R., Malanushenko, V., Malanushenko, E., Mao, S., Maraston, C., McDermid, R.M., Merrifield, M.R., Nichol, R.C., Oravetz, D., Pan, K., Parejko, J.K., Sanchez, S.F., Schlegel, D., Simmons, A., Steele, O., Steinmetz, M., Thanjavur, K., Thompson, B.A., Tinker, J.L., van den Bosch, R.C.E., Westfall, K.B., Wilkinson, D., Wright, S., Xiao, T., Zhang, K., 2015. Overview of the SDSS-IV MaNGA Survey: Mapping nearby Galaxies at Apache Point Observatory. *ApJ* 798, 7. doi:10.1088/0004-637X/798/1/7, arXiv:1412.1482.
- Cappellari, M., Copin, Y., 2003. Adaptive spatial binning of integral-field spectroscopic data using Voronoi tessellations. *MNRAS* 342, 345–354. doi:10.1046/j.1365-8711.2003.06541.x, arXiv:astro-ph/0302262.
- Conroy, C., 2013. Modeling the Panchromatic Spectral Energy Distributions of Galaxies. *ARA&A* 51, 393–455. doi:10.1146/annurev-astro-082812-141017, arXiv:1301.7095.
- de Blok, W.J.G., Walter, F., Brinks, E., Trachternach, C., Oh, S.H., Kennicutt, R. C., J., 2008. High-Resolution Rotation Curves and Galaxy Mass Models from THINGS. *AJ* 136, 2648–2719. doi:10.1088/0004-6256/136/6/2648, arXiv:0810.2100.
- Di Valentino, E., Mena, O., Pan, S., Visinelli, L., Yang, W., Melchiorri, A., Mota, D.F., Riess, A.G., Silk, J., 2021. In the realm of the Hubble tension-a review of solutions. *Classical and Quantum Gravity* 38, 153001. doi:10.1088/1361-6382/ac086d, arXiv:2103.01183.
- Domínguez Sánchez, H., Huertas-Company, M., Bernardi, M., Tuccillo, D., Fischer, J.L., 2018. Improving galaxy morphologies for SDSS with Deep Learning. *MNRAS* 476, 3661–3676. doi:10.1093/mnras/sty338, arXiv:1711.05744.
- Domínguez Sánchez, H., Margalef, B., Bernardi, M., Huertas-Company, M., 2022. SDSS-IV DR17: final release of MaNGA PyMorph photometric and deep-learning morphological catalogues. *MNRAS* 509, 4024–4036. doi:10.1093/mnras/stab3089, arXiv:2110.10694.
- Famaey, B., McGaugh, S.S., 2012. Modified Newtonian Dynamics (MOND): Observational Phenomenology and Relativistic Extensions. *Living Reviews in Relativity* 15, 10. doi:10.12942/lrr-2012-10, arXiv:1112.3960.
- Graham, M.T., Cappellari, M., Li, H., Mao, S., Bershadsky, M.A., Bizyaev, D., Brinkmann, J., Brownstein, J.R., Bundy, K., Drory, N., Law, D.R., Pan, K., Thomas, D., Wake, D.A., Weijmans, A.M., Westfall, K.B., Yan, R., 2018. SDSS-IV MaNGA: stellar angular momentum of about 2300 galaxies: unveiling the bimodality of massive galaxy properties. *MNRAS* 477, 4711–4737. doi:10.1093/mnras/sty504, arXiv:1802.08213.
- Hibat-Allah, M., Melko, R.G., Carrasquilla, J., 2023. Investigating topological order using recurrent neural networks. *Phys. Rev. B* 108, 075152. doi:10.1103/PhysRevB.108.075152, arXiv:2303.11207.
- Huang, F., Li, Y.Z., Yu, J.H., 2024. Distinguishing thermal histories of dark matter from structure formation. *J. Cosmology Astropart. Phys.* 2024, 023. doi:10.1088/1475-7516/2024/01/023, arXiv:2306.00065.
- Hubble, E.P., 1927. The classification of spiral nebulae. *The Observatory* 50, 276–281.
- Jedamzik, K., Pogosian, L., Zhao, G.B., 2021. Why reducing the cosmic sound horizon alone can not fully resolve the Hubble tension. *Communications Physics* 4, 123. doi:10.1038/s42005-021-00628-x, arXiv:2010.04158.
- Ku, H.H., 1966. Notes on the use of propagation of error formulas. *J. Res. Nat. B. Stand.* 70C, 262. doi:10.6028/jres.070c.025.
- Lelli, F., McGaugh, S.S., Schombert, J.M., 2016. SPARC: Mass Models for 175 Disk Galaxies with Spitzer Photometry and Accurate Rotation Curves. *AJ* 152, 157. doi:10.3847/0004-6256/152/6/157, arXiv:1606.09251.
- Lu, S., Zhu, K., Cappellari, M., Li, R., Mao, S., Xu, D., 2023. MaNGA DynPop - II. Global stellar population, gradients, and star-formation histories from integral-field spectroscopy of 10K galaxies: link with galaxy rotation, shape, and total-density gradients. *MNRAS* 526, 1022–1045. doi:10.1093/mnras/stad2732, arXiv:2304.11712.
- Lu, S., Zhu, K., Cappellari, M., Li, R., Mao, S., Xu, D., 2024. MaNGA DynPop - V. The dark-matter fraction versus stellar velocity dispersion relation and stellar

- initial mass function variations in galaxies: dynamical models and full spectrum fitting of integral-field spectroscopy. MNRAS 530, 4474–4492. doi:10.1093/mnras/stae1116, arXiv:2309.12395.
- Madau, P., Dickinson, M., 2014. Cosmic Star-Formation History. ARA&A 52, 415–486. doi:10.1146/annurev-astro-081811-125615, arXiv:1403.0007.
- Maslej-Krešňáková, V., El Boucheiry, K., Butka, P., 2021. Morphological classification of compact and extended radio galaxies using convolutional neural networks and data augmentation techniques. MNRAS 505, 1464–1475. doi:10.1093/mnras/stab1400, arXiv:2107.00385.
- McGaugh, S.S., 2012. The Baryonic Tully-Fisher Relation of Gas-rich Galaxies as a Test of Λ CDM and MOND. AJ 143, 40. doi:10.1088/0004-6256/143/2/40, arXiv:1107.2934.
- McGaugh, S.S., Lelli, F., Schombert, J.M., 2016. Radial Acceleration Relation in Rotationally Supported Galaxies. Phys. Rev. Lett. 117, 201101. doi:10.1103/PhysRevLett.117.201101, arXiv:1609.05917.
- McGaugh, S.S., Schombert, J.M., Bothun, G.D., de Blok, W.J.G., 2000. The Baryonic Tully-Fisher Relation. ApJ 533, L99–L102. doi:10.1086/312628, arXiv:astro-ph/0003001.
- Medina-Rosales, E., Cabrera-Vives, G., Miller, C.J., 2024. Mitigating bias in deep learning: training unbiased models on biased data for the morphological classification of galaxies. MNRAS 531, 52–60. doi:10.1093/mnras/stae1088, arXiv:2308.11007.
- Milgrom, M., 1983. A modification of the Newtonian dynamics as a possible alternative to the hidden mass hypothesis. ApJ 270, 365–370. doi:10.1086/161130.
- Natarajan, P., Williams, L.L.R., Bradač, M., Grillo, C., Ghosh, A., Sharon, K., Wagner, J., 2024. Strong Lensing by Galaxy Clusters. Space Sci. Rev. 220, 19. doi:10.1007/s11214-024-01051-8, arXiv:2403.06245.
- Ndung'u, S., Grobler, T., Wijnholds, S.J., Karastoyanova, D., Azzopardi, G., 2023. Advances on the morphological classification of radio galaxies: A review. New A Rev. 97, 101685. doi:10.1016/j.newar.2023.101685.
- Nestor Shachar, A., Price, S.H., Förster Schreiber, N.M., Genzel, R., Shimizu, T.T., Tacconi, L.J., Übler, H., Burkert, A., Davies, R.I., Dekel, A., Herrera-Camus, R., Lee, L.L., Liu, D., Lutz, D., Naab, T., Neri, R., Renzini, A., Saglia, R., Schuster, K.F., Sternberg, A., Wisnioski, E., Wuyts, S., 2023. RC100: Rotation Curves of 100 Massive Star-forming Galaxies at $z = 0.6\text{--}2.5$ Reveal Little Dark Matter on Galactic Scales. ApJ 944, 78. doi:10.3847/1538-4357/aca9cf, arXiv:2209.12199.
- Oh, S.H., Staveley-Smith, L., Spekkens, K., Kamphuis, P., Koribalski, B.S., 2018. 2D Bayesian automated tilted-ring fitting of disc galaxies in large H I galaxy surveys: 2DBAT. MNRAS 473, 3256–3298. doi:10.1093/mnras/stx2304, arXiv:1709.02049.
- Perivolaropoulos, L., Skara, F., 2022. Challenges for Λ CDM: An update. New A Rev. 95, 101659. doi:10.1016/j.newar.2022.101659, arXiv:2105.05208.
- Pilyugin, L.S., Grebel, E.K., Zinchenko, I.A., Nefedyev, Y.A., Vlchez, J.M., 2019. Relations between abundance characteristics and rotation velocity for star-forming MaNGA galaxies. A&A 623, A122. doi:10.1051/0004-6361/201834239, arXiv:1901.11001.
- Pilyugin, L.S., Grebel, E.K., Zinchenko, I.A., Vlchez, J.M., Sakhov, F., Nefedyev, Y.A., Berczik, P.P., 2020. Properties of galaxies with an offset between the position angles of the major kinematic and photometric axes. A&A 634, A26. doi:10.1051/0004-6361/201936357, arXiv:1912.03233.
- Riess, A.G., Yuan, W., Macri, L.M., Scolnic, D., Brout, D., Casertano, S., Jones, D.O., Murakami, Y., Anand, G.S., Breuval, L., Brink, T.G., Filippenko, A.V., Hoffmann, S., Jha, S.W., D'arcy Kenworthy, W., Mackenty, J., Stahl, B.E., Zheng, W., 2022. A Comprehensive Measurement of the Local Value of the Hubble Constant with $1 \text{ km s}^{-1} \text{ Mpc}^{-1}$ Uncertainty from the Hubble Space Telescope and the SH0ES Team. ApJ 934, L7. doi:10.3847/2041-8213/ac5c5b, arXiv:2112.04510.
- Rubin, V.C., Ford, W. Kent, J., 1970. Rotation of the Andromeda Nebula from a Spectroscopic Survey of Emission Regions. ApJ 159, 379. doi:10.1086/150317.
- Salpeter, E.E., 1955. The Luminosity Function and Stellar Evolution. ApJ 121, 161. doi:10.1086/145971.
- Sanders, R.H., McGaugh, S.S., 2002. Modified Newtonian Dynamics as an Alternative to Dark Matter. ARA&A 40, 263–317. doi:10.1146/annurev.astro.40.060401.093923, arXiv:astro-ph/0204521.
- Slipher, V.M., 1915. Spectrographic Observations of Nebulae. Popular Astronomy 23, 21–24.
- Stone, C., Courteau, S., Arora, N., 2021. The Intrinsic Scatter of Galaxy Scaling Relations. ApJ 912, 41. doi:10.3847/1538-4357/abebe4, arXiv:2104.07034.
- Tristram, M., Banday, A.J., Douspis, M., Garrido, X., Górski, K.M., Henrot-Versillé, S., Hergt, L.T., Ilić, S., Keskitalo, R., Lagache, G., Lawrence, C.R., Partridge, B., Scott, D., 2024. Cosmological parameters derived from the final Planck data release (PR4). A&A 682, A37. doi:10.1051/0004-6361/202348015, arXiv:2309.10034.
- Tully, R.B., Fisher, J.R., 1977. A new method of determining distances to galaxies. A&A 54, 661–673.
- van Putten, M.H.P.M., 2017a. Anomalous Galactic Dynamics by Collusion of Rindler and Cosmological Horizons. ApJ 837, 22. doi:10.3847/1538-4357/aa5da9.
- van Putten, M.H.P.M., 2017b. Evidence for Galaxy Dynamics Tracing Background Cosmology Below the de Sitter Scale of Acceleration. ApJ 848, 28. doi:10.3847/1538-4357/aa8cc, arXiv:1709.05944.
- van Putten, M.H.P.M., 2018. Self-similar galaxy dynamics below the de Sitter scale of acceleration. MNRAS 481, L26–L29. doi:10.1093/mnrasl/sly149, arXiv:1804.06212.
- van Putten, M.H.P.M., 2021. Evidence of the fine-structure constant in H_0 -tension. Physics Letters B 823, 136737. doi:10.1016/j.physletb.2021.136737.
- van Putten, M.H.P.M., 2024a. Galaxy dynamics tracing quantum cosmology beyond Λ CDM below the de Sitter scale of acceleration. Chinese Journal of Physics 91, 377–381. doi:10.1016/j.cjph.2024.07.040, arXiv:2408.06399.
- van Putten, M.H.P.M., 2024b. The Fast and Furious in JWST high- z galaxies. Physics of the Dark Universe 43, 101417. doi:10.1016/j.dark.2023.101417, arXiv:2312.16692.
- van Putten, M.H.P.M., 2025. On the Hubble expansion in a Big Bang quantum cosmology. Journal of High Energy Astrophysics 45, 194–199. doi:10.1016/j.jheap.2024.12.002, arXiv:2403.10865.
- Warner, P.J., Wright, M.C.H., Baldwin, J.E., 1973. High resolution observations of neutral hydrogen in M33 - II. The velocity field. MNRAS 163, 163. doi:10.1093/mnras/163.2.163.
- Westfall, K.B., Cappellari, M., Bershady, M.A., Bundy, K., Belfiore, F., Ji, X., Law, D.R., Schaefer, A., Shetty, S., Tremonti, C.A., Yan, R., Andrews, B.H., Brownstein, J.R., Cherinka, B., Coccato, L., Drory, N., Maraston, C., Parikh, T., Sánchez-Gallego, J.R., Thomas, D., Weijmans, A.M., Barrera-Ballesteros, J., Du, C., Goddard, D., Li, N., Masters, K., Ibarra Medel, H.J., Sánchez, S.F., Yang, M., Zheng, Z., Zhou, S., 2019. The Data Analysis Pipeline for the SDSS-IV MaNGA IFU Galaxy Survey: Overview. AJ 158, 231. doi:10.3847/1538-3881/ab44a2, arXiv:1901.00856.
- Yan, R., Chen, Y., Lazarz, D., Bizyaev, D., Maraston, C., Springfellow, G.S., McCarthy, K., Meneses-Goytia, S., Law, D.R., Thomas, D., Falcon Barroso, J., Sánchez-Gallego, J.R., Schlafly, E., Zheng, Z., Argudo-Fernández, M., Beaton, R.L., Beers, T.C., Bershady, M., Blanton, M.R., Brownstein, J., Bundy, K., Chambers, K.C., Cherinka, B., De Lee, N., Drory, N., Galbany, L., Holtzman, J., Imig, J., Kaiser, N., Kinemuchi, K., Liu, C., Luo, A.L., Magnier, E., Majewski, S., Nair, P., Oravetz, A., Oravetz, D., Pan, K., Sobeck, J., Stassun, K., Talbot, M., Tremonti, C., Waters, C., Weijmans, A.M., Wilhelm, R., Zasowski, G., Zhao, G., Zhao, Y.H., 2019. SDSS-IV MaStar: A Large and Comprehensive Empirical Stellar Spectral Library—First Release. ApJ 883, 175. doi:10.3847/1538-4357/ab3ebc, arXiv:1812.02745.
- Zhang, Y., Golden-Marx, J.B., Ogando, R.L.C., Yanny, B., Rykoff, E.S., Allam, S., Aguena, M., Bacon, D., Bocquet, S., Brooks, D., Carnero Rosell, A., Carretero, J., Cheng, T.Y., Conselice, C., Costanzi, M., da Costa, L.N., Pereira, M.E.S., Davis, T.M., Desai, S., Diehl, H.T., Doel, P., Ferrero, I., Flaugher, B., Frieman, J., Gruen, D., Gruendl, R.A., Hinton, S.R., Hollowood, D.L., Honscheid, K., James, D.J., Jeltema, T., Kuehn, K., Kuropatkin, N., Lahav, O., Lee, S., Lima, M.,

- Mena-Fernández, J., Miquel, R., Palmese, A., Pieres, A., Plazas Malagón, A.A., Romer, A.K., Sanchez, E., Smith, M., Suchyta, E., Tarle, G., To, C., Tucker, D.L., Weaverdyck, N., DES Collaboration, 2024. Dark Energy Survey Year 6 results: Intra-cluster light from redshift 0.2 to 0.5. *MNRAS* 531, 510–529. doi:10.1093/mnras/stae1165, arXiv:2309.00671.
- Zibetti, S., Charlot, S., Rix, H.W., 2009. Resolved stellar mass maps of galaxies - I. Method and implications for global mass estimates. *MNRAS* 400, 1181–1198. doi:10.1111/j.1365-2966.2009.15528.x, arXiv:0904.4252.
- Zwicky, F., 1937. On the Masses of Nebulae and of Clusters of Nebulae. *ApJ* 86, 217. doi:10.1086/143864.

SUPPORTING INFORMATION

Supplementary data on Δ_b PA are available online.